JOURNAL OF AIRCRAFT
Vol. 33, No. 4, July–August 1996

Finite Element Analysis of a Samara-Wing Decelerator

Peter Crimi*
Andover Applied Sciences, Inc., North Andover, Massachusetts 01845

An analytic model of a samara-wing decelerator has been developed that employs a finite element representation of the fabric wing. A method has been derived for iteratively calculating the steady-state descent characteristics from the equations of motion of the system, which is composed of the 12 rigid-body degrees of freedom of the centerbody and tip mass together with the translational degrees of freedom of the fabric nodal masses. Results of calculations are compared with the measured descent characteristics of both full-scale submunition simulators and subscale wind-tunnel test articles. Agreement between analysis and test results is generally quite good, but failure to predict spin rate in certain cases indicates the need for further fabric modeling effort.

Nomenclature

c	= wing chord
d	= section drag/unit span
E_f	= fabric modulus, force/unit length
F_{fX_i}, F_{fY_i}, F_{fZ_i}	= nodal force components, $i = 1, 2, \ldots, N_f$
F_{x_i}, F_{y_i}, F_{z_i}	= applied force components, $i = 1, 2$
G_i	= iteration function
h_{x_i}, h_{y_i}, h_{z_i}	= angular momentum components, $i = 1, 2$
k_c, k_s	= chordwise, spanwise element stiffness
l	= section lift/unit span
M_f'	= fabric mass/unit area
M_{x_i}, M_{y_i}, M_{z_i}	= applied moment components, $i = 1, 2$
m_f	= nodal mass
m_1, m_2	= centerbody, tip mass
N_c, N_s	= number of chordwise, spanwise elements
N_f	= number of fabric nodal masses
N_T	= total number of variables defining steady descent
q_i	= iteration variable
s	= wingspan
T	= wing or rotor thrust
V	= total relative air velocity magnitude
V_s	= sink rate
V_T, V_N	= flow components caused by wing motion
w_{CB}	= interference flow caused by centerbody
w_i	= wake-induced inflow
X, Y, Z	= inertial coordinates, Z vertical
x_i, y_i, z_i	= body-fixed coordinates, $i = 1, 2$
y_w, z_w	= wing attachment radial, axial offset
α	= section angle of attack
δ_X, δ_Y	= center-of-rotation offsets from centerbody c.g.
ρ	= air density
τ	= chord line inclination
ψ_i, θ_i, ϕ_i	= Euler angles, $i = 1, 2$
Ω	= angular velocity magnitude
ω_{x_i}, ω_{y_i}, ω_{z_i}	= angular velocity components, $i = 1, 2$

Introduction

A SAMARA-WING decelerator is a device that controls the descent rate of a sensor-fused submunition while imparting a coning lunar rotation to provide a regular scanning pattern for the sensor. The decelerator is simply a rectangular fabric wing attached to the top of the cylindrical submunition and formed into an aerodynamic surface by the centrifugal load on a small mass attached to the tip of the wing. By causing the submunition to autorotate in steady descent, its role is analogous to that of a maple or elm seed wing, from which the term samara is derived.

The function of this device has been demonstrated in several series of tests in vertical wind tunnels.[1–3] These tests primarily employed subweight, subscale test articles. More recently, cable-drop tests of samara wings on full-scale submunition simulators were conducted.[4] Steady descent characteristics were measured for several different wing planforms, and the transition to steady descent following simulated release from a carrier vehicle was sucessfully demonstrated during these tests.

Samara-wing decelerators have been the subject of several analytic studies. An aeroballistic simulation computer program was employed by Kline and Koenig[3] to define flight characteristics using empirically derived aerodynamic coefficients. In Ref. 5, an analytic model of a submunition employing a samara wing was developed with aerodynamic loading computed using a strip assumption. Seven degrees of freedom, including the flapping response of a rigid wing, were modeled. The aeroelastic response of the system was incorporated in the formulations of Ref. 6, where the samara wing was modeled by four elastic cords connecting the centerbody to the tip mass. This model formed the basis for a method of calculating the steady-state descent characteristics.

Results from the analysis method of Ref. 6 were in fairly good agreement with wind-tunnel test measurements on subweight models, but pretest predictions did not agree well with the results of the drop tests with full-scale submunition simulators reported in Ref. 4. The test results indicated that the wings develop considerably more aerodynamic load than is predicted using flat-plate aerodynamic coefficients for the wing section. After empirically adjusting the wing section coefficients, calculated results were in good agreement with the test measurements, and so the analysis method could be used to define a wing design for the configuration tested.

This experience motivated the development of a refined analytic model of the samara wing. It was decided to provide a better representation of the coupling between the wing response and aerodynamic loading by employing a finite element fabric model. The method for determining the solution of the equations of motion for steady-state descent is similar to that of Ref. 6, but modified to accommodate the greatly increased number of degrees of freedom. The specific formulations used and the results of computations are presented in the following text.

Received Jan. 28, 1995; revision received Jan. 12, 1996; accepted for publication Jan. 12, 1996.

*President, P.O. Box 578. Senior Member AIAA.

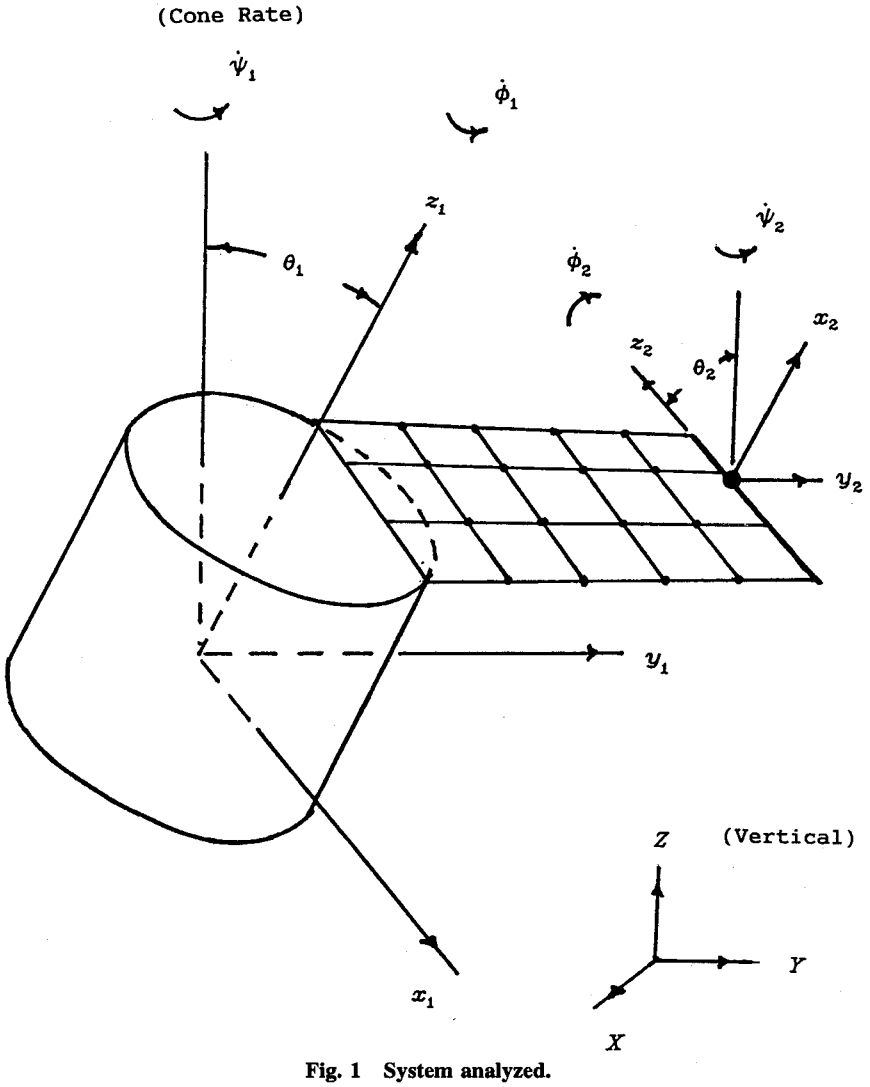

Fig. 1 System analyzed.

Formulations

System Analyzed

The system analyzed consists of a cylindrical centerbody, a rod-shaped tip mass, and a finite element representation of the fabric wing constructed from a mesh of elastic cords connected to nodal masses, as shown in Fig. 1.

With regard to the wing model, at any spanwise section there are N_c equally spaced chordwise elements, and at any chordwise section there are N_s equally spaced spanwise elements. The chordwise elements are positioned so that they are at the midpoints of N_c chordwise strips of equal width s/N_c. The total aerodynamic load on each chordwise strip is apportioned to the nodal masses on that strip in such a way as to produce the correct c.p. If c is the wing chord and M_f' is the fabric mass per unit area, the nodal masses are all assigned the same values, given by

$$m_f = \frac{M_f' sc}{N_s N_c}$$

The nodal masses on the leading and trailing edges would be half those of interior nodes if the fabric were of uniform thickness, because the edge nodes take on the mass of just half an element width. The leading and trailing edges are hemmed, however, so that it is not unreasonable to make all nodal masses equal. To assign element stiffnesses, let E_f be the fabric modulus, with units of force per unit length. With all chordwise elements having equal stiffness, it follows that their values should be

$$k_c = \frac{E_f s(N_s - 1)}{cN_c}$$

With the leading and trailing edges hemmed, it is again not unreasonable to make all spanwise elements of equal stiffness as well, from which it follows that

$$k_s = \frac{E_f cN_c}{sN_s}$$

for all but the elements attached to the centerbody or tip mass. Those elements are half as long as the others, and so they are twice as stiff.

Equations of Motion

For the formulation of the equations of motion, body-fixed coordinate systems (x_1, y_1, z_1) and (x_2, y_2, z_2) are used with origins at the mass center of the centerbody and tip mass, respectively, as indicated in Fig. 1. Angular displacements of those coordinate systems are measured by Euler angles referred to inertial coordinates (X, Y, Z), Z being vertical. The order of the rotations to form the Euler angles for, say, the centerbody is first about z_1, to define ψ_1, then about x_1, to define θ_1, and finally about z_1 again to define ϕ_1 (see Fig. 1). Note that in steady lunar rotation, the cone angle θ_1 is constant, while the rate of change of ψ_1, which is the precession rate, is

constant and equal to the spin rate, and ϕ_1 is also constant with a value near 180 deg, which results in the wing extending radially outward.

Let h_{x_i}, h_{y_i}, and h_{z_i} denote the components of angular momentum of the centerbody and tip mass, and let ω_{x_i}, ω_{y_i}, and ω_{z_i} denote the corresponding angular velocity components. The angular momentum components are given by

$$h_x = I_{xx}\omega_x + I_{xy}\omega_y + I_{xz}\omega_z$$

$$h_y = I_{xy}\omega_x + I_{yy}\omega_y + I_{yz}\omega_z$$

$$h_z = I_{xz}\omega_z + I_{yz}\omega_y + I_{zz}\omega_z$$

with i subscripts understood on all x, y, and z, I_{xx}, I_{xy}, etc., being the moments and products of inertia of the two bodies. The 12 equations of motion for the centerbody and tip mass are (with $i = 1$ for the centerbody and 2 for the tip mass)

$$\dot{h}_{x_i} = \omega_{z_i}h_{y_i} - \omega_{y_i}h_{z_i} + M_{x_i} \tag{1}$$

$$\dot{h}_{y_i} = \omega_{x_i}h_{z_i} - \omega_{z_i}h_{x_i} + M_{y_i} \tag{2}$$

$$\dot{h}_{z_i} = \omega_{y_i}h_{x_i} - \omega_{x_i}h_{y_i} + M_{z_i} \tag{3}$$

$$m_i\ddot{X}_i = F_{X_i} \tag{4}$$

$$m_i\ddot{Y}_i = F_{Y_i} \tag{5}$$

$$m_i\ddot{Z}_i = F_{Z_i} \tag{6}$$

where M_{x_i}, M_{y_i}, and M_{z_i} are moment components about body-fixed axes and F_{X_i}, F_{Y_i}, and F_{Z_i} are force components in the inertial frame, while m_1 and m_2 are the masses of the centerbody and tip mass, respectively.

Finally, if there are N_f fabric masses, their $3N_f$ equations of motion are (for $i = 1, 2, \ldots, N_f$)

$$m_f\ddot{X}_{f_i} = F_{fX_i} \tag{7}$$

$$m_f\ddot{Y}_{f_i} = F_{fY_i} \tag{8}$$

$$m_f\ddot{Z}_{f_i} = F_{fZ_i} \tag{9}$$

Force and Moment Evaluations

The contributions to the force and moment components from each elastic cord are evaluated by calculating the strain in the cord, multiplying by the appropriate stiffness to obtain the magnitude of the tensile force, and determining the direction of the force from the locations of the endpoints.

The aerodynamic loading on the centerbody is computed using coefficients extracted from appropriate test data.[7,8] The axial and normal force coefficients obtained are plotted in Fig. 2, the angle of attack being measured from the cylinder axis.

To compute the aerodynamic loading on the samara wing, the load on each chordwise strip is evaluated separately. For each strip, a chord line is defined that connects the nodal masses on the leading and trailing edges, and a local normal to the fabric is defined by the lines connecting adjacent nodal masses in the spanwise direction. The local aerodynamic loading is assumed to act in the plane of that normal and the chord line. The velocities of the nodal masses on the leading and trailing edges are then averaged, and the components of that average in the plane of the wing section are computed. The situation in the plane normal to the wing is as shown in Fig. 3. The wing section sees a horizontal flow component V_T caused by its own velocity and a component $V_N - w_i + w_{CB}$ normal to it, where V_N is the contribution of the wing section velocity, w_i is the inflow induced by the wake of the samara

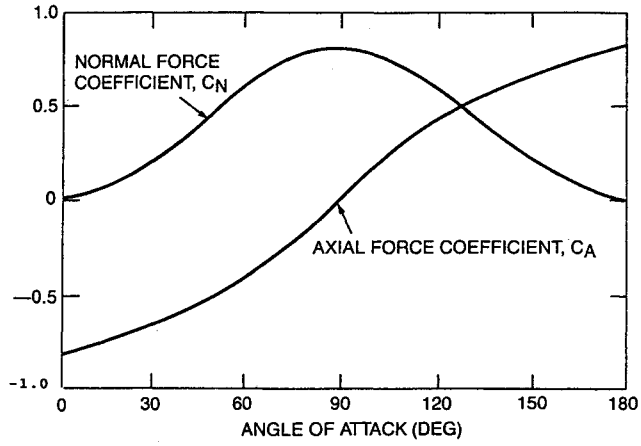

Fig. 2 Centerbody aerodynamic coefficients.

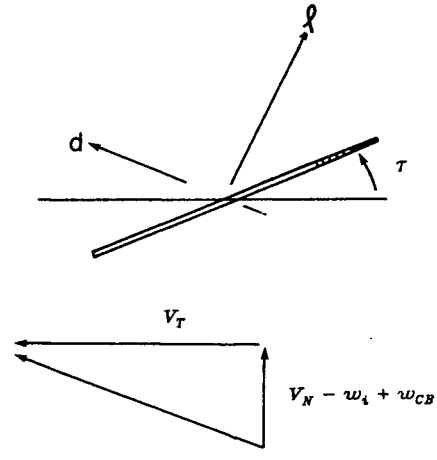

Fig. 3 Relative flow and loading at a wing section.

wing, and w_{CB} is the interference flow produced by the centerbody. Concerning w_i, the wing is generally operating as a helicopter rotor when in the so-called windmill-brake state. In that case, the inflow can be obtained in terms of the rotor thrust T, using momentum considerations, with the result that (Ref. 9)

$$w_i = \frac{V_s}{2} - \left[\left(\frac{V_s}{2}\right)^2 - \frac{T}{2\pi(y_w + s)^2}\right]^{1/2}$$

where y_w is the wing attachment radial offset from the z_1 axis. In place of rotor thrust in this formula, 0.9 times the total vehicle weight was substituted to evaluate samara-wing-induced inflow, the drag on the centerbody being about 10% of the total weight in most cases.

Concerning w_{CB}, a bluff body produces a locally accelerated flow in the freestream direction. In the absence of any directly applicable data, flow measurements in the vicinity of a disk held normal to the flow reported in Ref. 10 were used. Those data show a variation of w_{CB} with radial distance r of

$$w_{CB}/V_s \approx (R/r)^{1.7}, \qquad (r/R) \geq 1.8$$

where R is disk radius. Measurements were not taken for r/R less than 1.8, and so the value at 1.8 was used for all inboard points. For an effective disk radius, the distance from the centerbody mass center to the wing attachment was used, i.e., $R = \sqrt{y_w^2 + z_w^2}$, z_w being the axial offset of the wing attachment.

With the local flow defined, the section incidence α is computed according to

$$\alpha = \tau + \tan^{-1}\left(\frac{V_N - w_i + w_{CB}}{V_T}\right)$$

where τ is the local inclination of the chord line with respect to the horizontal in the wing section plane (see Fig. 3). With section lift and drag coefficients defined as functions of α, the lift l and drag d per unit span are then given by

$$l = (\rho/2)V^2cC_l(\alpha)$$

$$d = (\rho/2)V^2cC_d(\alpha)$$

where $V^2 = V_T^2 + (V_N - w_i + w_{CB})^2$.

The variations of C_l, C_d, and the c.p. with α were taken from wind-tunnel measurements on an NACA 0012 airfoil section at incidence angles from 0 to 180 deg (Ref. 11). Since the samara wing has a sharp leading edge, the measured data were shifted 180 deg in α, making the stall characteristics the same as those of an airfoil in reversed flow. Data from flat-plate or fabric measurements would have been preferred, but none could be found with both c.p. measurements and angles of attack well above stall. The section coefficients used are plotted in Fig. 4.

To apportion the total aerodynamic load on a chordwise strip to the N_s nodal masses on that strip, the normal and in-plane components are calculated, and the in-plane component is divided equally among the masses on the strip. The normal component is apportioned by assuming the nodal loads vary linearly in the chordwise direction, with the resultant of the nodal loads made to act at the c.p.

Method of Solution

For given centerbody, wing and tip mass geometries and inertial properties, the steady-state descent parameters are obtained by iteratively varying the dependent variables to satisfy the equations of motion. That is, the dependent variables of the physical system become the independent variables of the iteration process. To identify an appropriate set of variables, the conditions for steady descent must be imposed analytically.

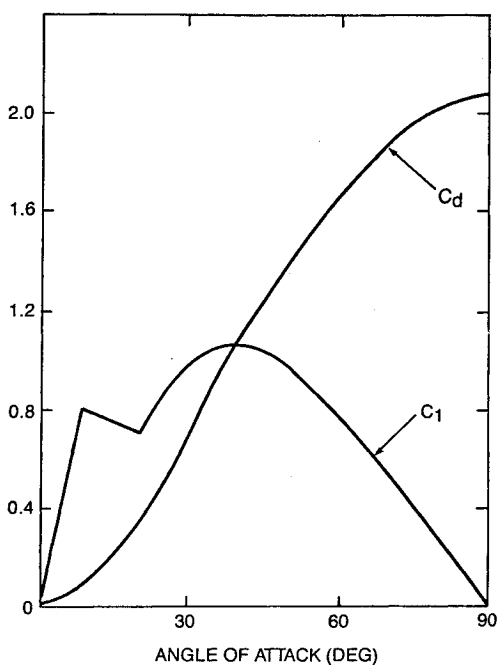

Fig. 4 Wing section lift and drag coefficients.

For this purpose, consider the differential equations for the centerbody Euler angles, given by

$$\dot{\psi}_1 = (\omega_{x_1} \sin \phi_1 + \omega_{y_1} \cos \phi_1)/\sin \theta_1$$

$$\dot{\phi}_1 = \omega_{z_1} - (\omega_{x_1} \sin \phi_1 + \omega_{y_1} \cos \phi_1)\cot \theta_1$$

$$\dot{\theta}_1 = \omega_{x_1} \cos \phi_1 - \omega_{y_1} \sin \phi_1$$

With steady lunar rotation, both $\dot{\phi}_1$ and $\dot{\theta}_1$ are zero and $\dot{\psi}_1$ is constant. Thus, it must be that

$$\phi_1 = \tan^{-1}(\omega_{x_1}/\omega_{y_1}) \tag{10}$$

$$\theta_1 = \tan^{-1}\left(\frac{\omega_{x_1} \sin \phi_1 + \omega_{y_1} \cos \phi_1}{\omega_{z_1}}\right) \tag{11}$$

$$\dot{\psi}_1 = \omega_{z_1} \sec \theta_1 \tag{12}$$

Therefore, specifying ω_{x_1}, ω_{y_1}, and ω_{z_1} completely defines the angular velocity and position of the centerbody in steady lunar rotation. To define the translational motion of the centerbody, it is necessary to specify the location of the center of rotation. Since the angular velocity vector is vertical, two coordinates are sufficient to define this point. With the mass center of the centerbody assumed to be instantaneously located at the origin of the inertial frame, the inertial coordinates of the center of rotation are denoted δ_X and δ_Y. The three inertial velocity components of the centerbody mass center are then given by

$$\dot{X}_1 = \Omega\delta_Y, \qquad \dot{Y}_1 = -\Omega\delta_X, \qquad \dot{Z}_1 = -V_s$$

The tip mass orientation and position relative to the centerbody define its motion. The six variables defining tip mass response are then the three Euler angles ψ_2, θ_2, and ϕ_2, and the three tip mass coordinates in the centerbody frame, denoted x_{1_t}, y_{1_t}, and z_{1_t}.

Lastly, the $3N_f$ inertial coordinates of the fabric nodal masses define their response. Note that the velocity components of nodal mass i are given by

$$\dot{X}_{f_i} = -\Omega(Y_{f_i} - \delta_Y), \qquad \dot{Y}_{f_i} = \Omega(X_{f_i} - \delta_X), \qquad \dot{Z}_{f_i} = -V_s$$

In summary, $N_T = 3N_f + 12$ variables completely define the response in steady descent. These are the three centerbody angular velocity components, the sink rate, the two coordinates of the center of rotation, the three tip mass Euler angles, the three tip mass coordinates, and the $3N_f$ fabric mass coordinates. From the equations of motion, the N_T requirements to be satisfied are that the rate of change of the six angular momentum components, $\dot{Z}_1$, $\dot{Z}_2$, and $\dot{Z}_{f_i}$, $i = 1, 2, \ldots, N_f$ all equal zero, and that $\dot{X}_1$, $\dot{Y}_1$, $\dot{X}_2$, $\dot{Y}_2$, $\dot{X}_{f_i}$, and $\dot{Y}_{f_i}$, $i = 1, 2, \ldots, N_f$ all equal the appropriate components of centripetal acceleration. Those accelerations are readily computed from the inertial coordinates. For example, those of the fabric masses are given by

$$A_{X_{f_i}} = -(X_{f_i} - \delta_X)\Omega^2, \qquad A_{Y_{f_i}} = -(Y_{f_i} - \delta_Y)\Omega^2$$

and similarly for the centerbody and tip mass.

The iterative procedure can be described analytically as follows. First, denote the N_T variables by q_i, where

$$q_1 = x_{1_t}, \qquad q_2 = y_{1_t}, \qquad q_3 = z_{1_t}$$

$$q_4 = \psi_2, \qquad q_5 = \phi_2, \qquad q_6 = \theta_2$$

$$q_7 = X_{f_1}, \qquad q_8 = Y_{f_1}, \qquad q_9 = Z_{f_1}$$

$$\ldots$$

$$q_{N_f+7} = \delta_X, \qquad q_{N_f+8} = \delta_Y, \qquad q_{N_f+9} = V_s$$

$$q_{N_f+10} = \omega_{x_1}, \qquad q_{N_f+11} = \omega_{y_1}, \qquad q_{N_f+12} = \omega_{z_1}$$

Next, denote the N_T functions that are to vanish by $G_i(q_1, q_2, \ldots, q_{N_T})$, where

$$G_1 = F_{X_2} - m_2 A_{X_2}, \quad G_2 = F_{Y_2} - m_2 A_{Y_2}, \quad G_3 = F_{Z_2}$$

$$G_4 = M_{x_2}, \quad G_5 = M_{y_2}, \quad G_6 = M_{z_2}$$

$$G_7 = F_{fX_1} - m_f A_{X_{f1}}, \quad G_8 = F_{fY_1} - m_f A_{Y_{f1}}, \quad G_9 = F_{fZ_1}$$

$$\ldots$$

$$G_{N_f+7} = F_{X_1} - m_1 A_{X_1}, \quad G_{N_f+8} = F_{Y_1} - m_1 A_{Y_1}, \quad G_{N_f+9} = F_{Z_1}$$

$$G_{N_f+10} = M_{X_1}, \quad G_{N_f+11} = M_{y_1}, \quad G_{N_f+12} = M_{z_1}$$

The requirements for steady descent can then be written as

$$G_i(q_1, q_2, \ldots, q_{N_T}) = 0, \qquad i = 1, 2, \ldots, N_T \tag{13}$$

Let q_i^k be a value of q_i near the value for steady descent. For convenience of notation, further let

$$G_{ik} = G_i(q_1^k, q_2^k, \ldots, q_{N_T}^k)$$

$$\left(\frac{\partial G_i}{\partial q_j}\right)_k = \frac{\partial G_i}{\partial q_j^k}(q_1^k, q_2^k, \ldots, q_{N_T}^k)$$

If q_j^{k+1} is the value of q_j for steady descent, then each of G_i can be expanded in a Taylor series to give

$$G_{i,k+1} = 0 \approx G_{ik} + \sum_{j=1}^{N_T} \left(\frac{\partial G_i}{\partial q_j}\right)_k (q_j^{k+1} - q_j^k)$$

$$i = 1, 2, \ldots, N_T$$

This provides a set of linear algebraic equations that can be solved for the $(k + 1)$th estimate of the solution, the equations being

$$\sum_{j+1}^{N_T} C_{ij} q_j^{k+1} = b_i, \qquad i = 1, 2, \ldots, N_T \tag{14}$$

where

$$C_{ij} = \left(\frac{\partial G_i}{\partial q_j}\right)_k$$

$$b_i = \sum_{j=1}^{N_T} C_{ij} q_{j_k} - G_{ik}$$

Equations (14) were used to iteratively solve for the values of the dependent variables in steady descent. The partial derivatives are evaluated numerically, according to

$$\frac{\partial G_i}{\partial q_j} = [G_i(q_1, q_2, \ldots, q_j + \varepsilon, \ldots) - G_i(q_1, q_2, \ldots, q_j - \varepsilon, \ldots)]/(2\varepsilon)$$

where ε is a small number, the appropriate value of which was found by experimentation.

To initiate the iteration for a particular configuration, estimated values are assigned to ω_{x_1}, ω_{y_1}, ω_{z_1}, V_s, and the wing flapping and twist angles. From these parameters, estimated tip mass position and orientation are calculated and fabric nodal masses are positioned by iteratively balancing an average restraining force with the centrifugal load on the tip mass. The main iteration then proceeds. This is divided into inner and outer iterations. The inner iteration is performed by fixing the values of ω_{x_1}, ω_{y_1}, ω_{z_1}, and V_s, and iterating on the other $N_T - 4$ variables. That is, with the centerbody angular velocity and sink rate fixed, the tip mass and wing nodal mass positions are found. When a solution for the inner iteration is obtained, all N_T equations are used to compute a new estimate of centerbody angular velocity and sink rate, as well as the other variables, to provide the starting values for the next inner iteration.

Convergence to the solution is quite rapid, provided the initial estimates for the q_j values are sufficiently close to those of the solution vector. In the absence of a good estimate of the solution, divergence of the iteration is prevented by taking a weighted average of q_j^k and q_j^{k+1} in place of q_j^{k+1} for each succeeding step. When the change between succeeding steps falls below a specified threshold, the value of q_j^{k+1} is used directly. The first inner iteration is the most difficult because the fabric nodal masses are not well positioned, and the nonlinearity caused by fabric cord elements going slack produces rather erratic changes in the variables from step to step. Typically, the first inner iteration may require 20–30 steps, whereas successive ones may only need three or four. With a good initial estimate, a solution is obtained in four or five outer iterations.

For example, consider the analysis of test 6 from Ref. 4, the parameters and results of which are detailed in the next section. The following values were assumed to start the iteration:

$$\omega_{x_1} = 4.68 \text{ rad/s}, \quad \omega_{y_1} = -28.5 \text{ rad/s}, \quad \omega_{z_1} = 63.0 \text{ rad/s}$$

$$V_s = 103 \text{ ft/s}$$

Initial positioning of the tip mass produced the following for flap angle and twist angle of the tip mass:

$$\beta_T = 33.3 \text{ deg}, \quad \tau_T = 2.35 \text{ deg}$$

The inner iteration converged in 11 steps, using an allowable relative error on the variables of 0.0005. The flap and twist angles at the tip were then 33.4 and 4.97 deg, respectively. For the start of the second inner iteration, using a weighting factor of 0.83, the following values were obtained for angular velocity and sink rate:

$$\omega_{x_1} = 5.65 \text{ rad/s}, \quad \omega_{y_1} = -31.9 \text{ rad/s}, \quad \omega_{z_1} = 69.3 \text{ rad/s}$$

$$V_s = 105 \text{ ft/s}$$

The second inner iteration converged in five steps, and the third in three steps. Just three outer iterations were required, the final values for angular velocity and sink rate being

$$\omega_{x_1} = 5.85 \text{ rad/s}, \quad \omega_{y_1} = -32.6 \text{ rad/s}, \quad \omega_{z_1} = 70.4 \text{ rad/s}$$

$$V_s = 106 \text{ ft/s}$$

Table 1 Centerbody mass properties for Ref. 4 test articles

Weight, lb	Axial c.g., inches from base	Roll inertia, slug-ft^2	Pitch inertia, slug-ft^2
31.4	3.27	0.0461	0.0482
20.1	3.31	0.0374	0.0400

Table 2 Samara wing parameters for Ref. 4 test articles

Test no.	Sublet weight, lb	Samara wing			
		Chord, in.	Span, in.	Tip wt, lb	Tip c.g., %c
1	20	4.75	19.1	0.238	35.0
3	20	4.75	13.2	0.354	38.4
4	31	7.20	21.1	0.282	35.6
5	31	4.75	21.0	0.155	34.5
6	31	7.20	16.5	0.282	35.6
8	31	4.75	18.3	0.315	37.4
9	31	7.20	13.0	0.282	35.6

Final flap and twist angles were 32.8 and 1.03 deg, respectively.

Results of Computations

The steady-state descent characteristics were calculated for the full-scale test articles of the steady-state drop tests reported in Ref. 4 and for the 4-lb test articles used in the wind-tunnel tests reported in Ref. 1. The latter results provide a measure of the validity of the analytical model for a range of system parameter values.

Addressing the results for the drop test articles first, samara wing and centerbody parameters for those tests are listed in Tables 1 and 2. The wing fabric for all of the tests was a high-modulus polyethylene weighing approximately 0.05 lb/ft^2. Fabric modulus was estimated to be 2×10^6 lb/ft. The finite element mesh employed five chords spanwise and 10 chordwise, for a total of 50 fabric nodal masses.

Analysis results for the drop tests are compared with the test results in Table 3. Results are listed so as to group similar test articles. The first two listed are for the heavier test article with 4.75-in. chord wing, the next three are also for the heavier test article, but with 7.2-in. chord wing, while the last two are for the 20-lb test article.

Details of the solution are shown in Figs. 5–7 for test 6 to provide some insight as to how the decelerator functions. The wing in flight is nearly planar, as indicated from the plots of wing midchord ordinate relative to the root attachment, in centerbody coordinates, and the section twist angle relative to the root attachment, positive leading edge up, shown in Fig. 5. The combined effects of the wing twist, the angular motion and the sink rate, which result in the section normal and tangential relative velocity components shown in Fig. 6, produce an angle of attack of 38 deg near the tip, increasing to 77 deg near the root. As indicated in Fig. 7, with separated flow over the whole wing, the section drag coefficient varies from about

Table 3 Comparison of calculated and measured descent conditions

Test no.	Spin rate, Hz		Sink rate, fps		Cone angle, deg	
	Calculated	Measured	Calculated	Measured	Calculated	Measured
5	11.09	19.0	121.7	100.0	12.1	24
8	9.18	9.36	129.3	116.0	19.4	27
4	9.37	9.07	98.3	95.4	20.1	28
6	12.38	10.8	105.8	105.0	25.2	30
9	16.68	10.1	114.7	114.0	28.2	24
1	8.79	15.3	98.5	77.0	19.3	31
1[a]	15.4	15.3	88.6	77.0	30.8	31
3	8.64	20.7	114.8	91.4	21.4	45
3[b]	20.7	20.7	103.9	91.4	34.8	45

[a]Calculated with tip c.g. at 27.2% chord. [b]Calculated with tip c.g. at 28.2% chord.

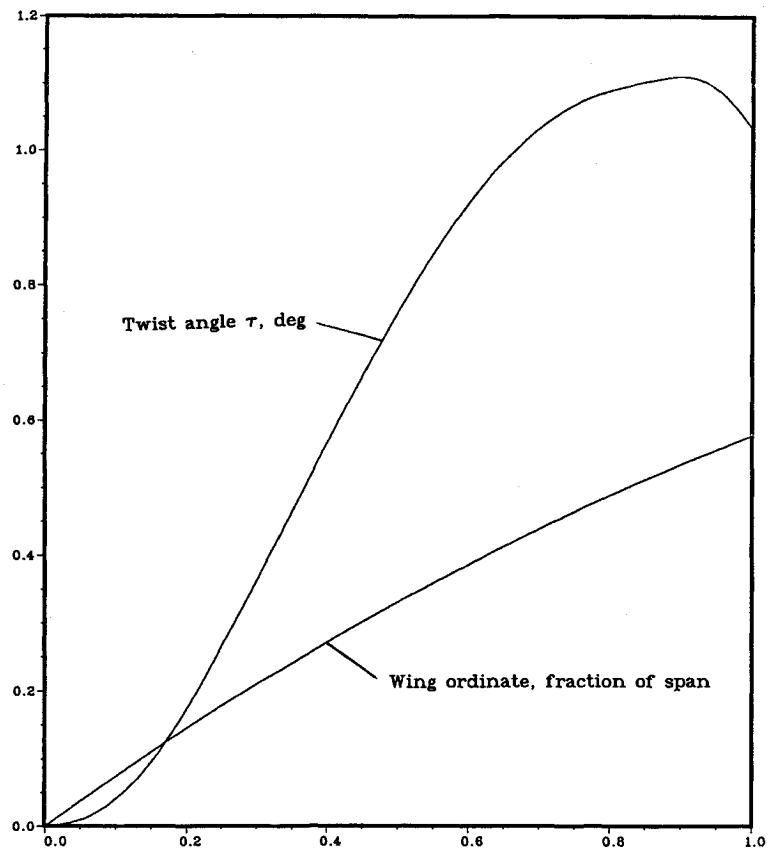

Fig. 5 Wing deformation, from analysis of test 6 (Ref. 4).

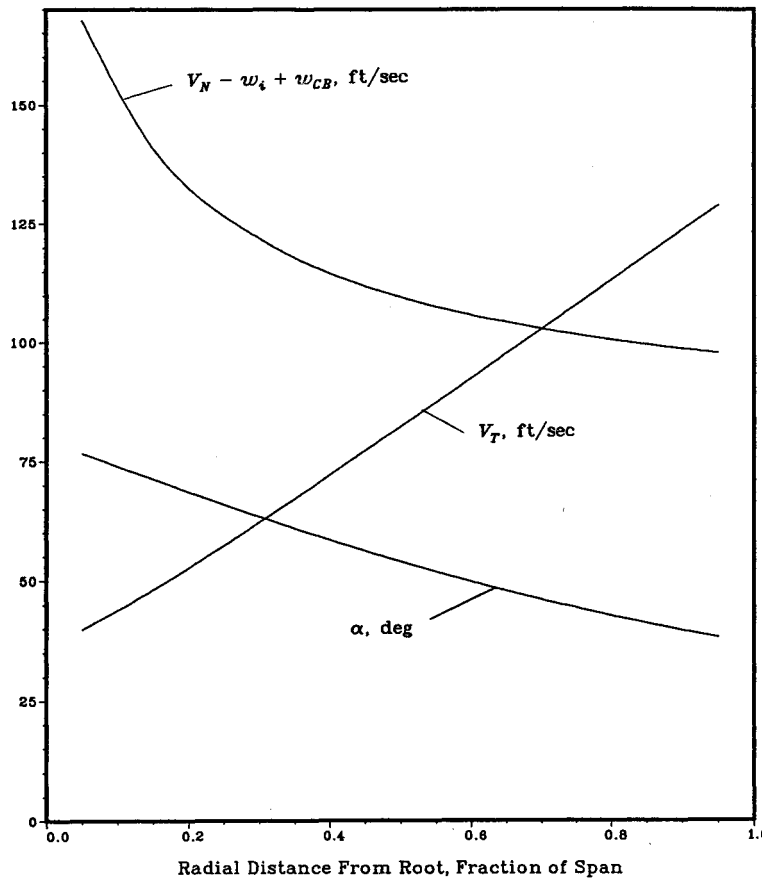

Fig. 6 Wing aerodynamic environment, from analysis of test 6 (Ref. 4).

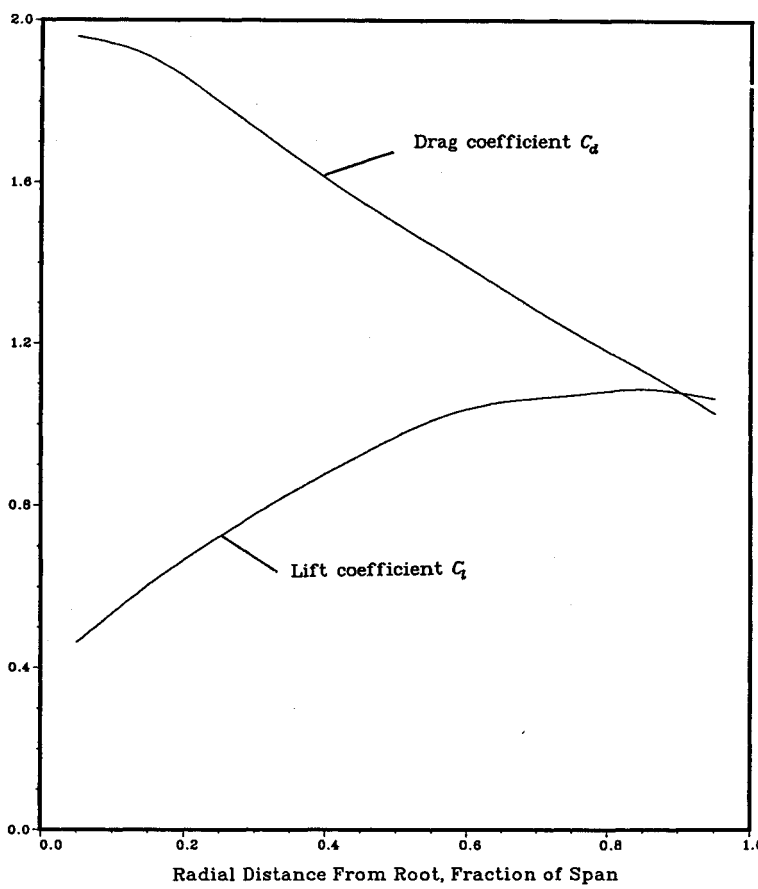

Fig. 7 Spanwise loading distribution, from analysis of test 6 (Ref. 4).

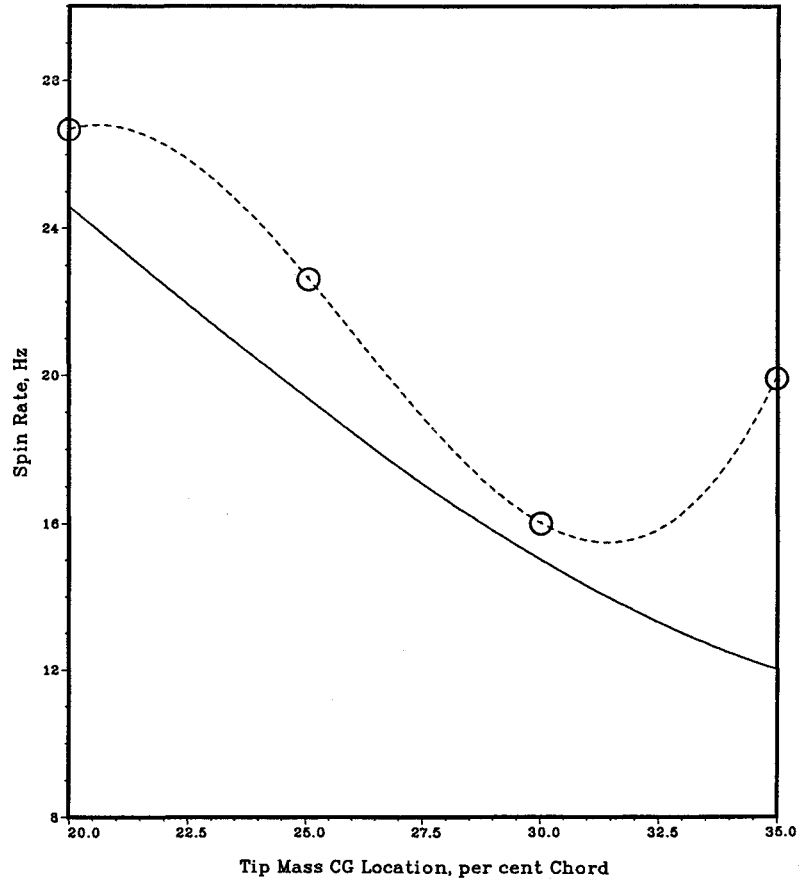

Fig. 8 Calculated (solid curve) and measured (dashed curve) spin rates (Ref. 1 tests).

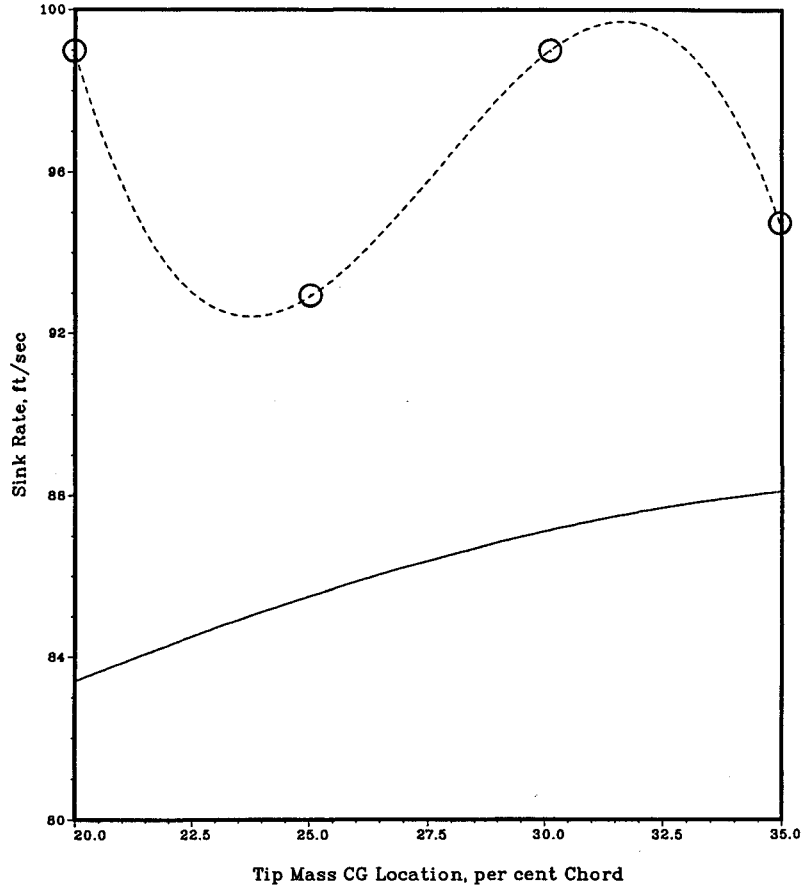

Fig. 9 Calculated (solid curve) and measured (dashed curve) sink rates (Ref. 1 tests).

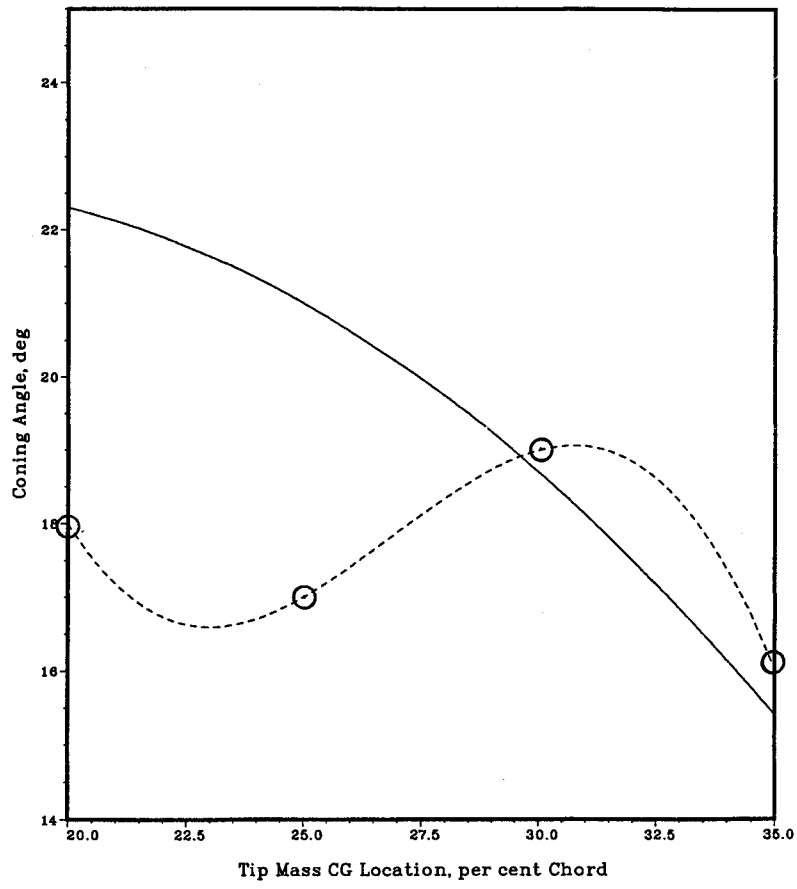

Fig. 10 Calculated (solid curve) and measured (dashed curve) coning angles (Ref. 1 tests).

one near the tip to two at the root, while the lift coefficient decreases from one at the tip to 0.5 at the root.

With regard to the results listed in Table 3, of the first five listed, all for the heavier test article, the results compare well for tests 8, 4, and 6, particularly with regard to spin rate and sink rate. The calculated spin rate for test 9 is 65% higher than what was measured, and for test 5 it is 37% low, causing the calculated sink rate to be 20% higher than what was measured. Of particular note for these five tests is that the predicted aerodynamic loading developed is roughly what was produced, in that when spin rates agree, so do sink rates. As noted earlier, the analysis results reported in Ref. 4 indicated that the samara wing was developing considerably more aerodynamic loading than was predicted. The improvement in this regard can be attributed to including the effects of the interference flow produced by the centerbody.

Results for the lighter test article, tests 1 and 3, are rather disappointing. The calculated spin rate for test 1 is 40% low, and for test 3 it is less than half the 20.7 Hz measured. The reason for this is not apparent, but a fairly modest forward shift of 8 or 9% of chord in the tip mass c.g. position brings the measured and calculated results into line, as indicated by the additional calculated results listed in Table 3.

Considering the tests reported in Ref. 1, the test articles weighed 4.0 lb, with a centerbody spin inertia of 0.00334 slug-ft^2 and a transverse inertia of 0.00395 slug-ft^2. The samara wings were Kevlar®, weighing 0.2 lb/ft^2 with an estimated modulus of 2 million lb/ft. For the four test articles analyzed, the wing chord was 3 in., the span was 5 in., and the tip mass weighed 0.1 lb. With the relatively low wing aspect ratio, only six chordwise elements, with again five spanwise elements, were used to represent the wing.

Analysis and test results are compared in Figs. 8, 9, and 10, where spin rate, sink rate, and cone angle, respectively, are plotted against tip mass c.g. position. The agreement for all three descent variables is quite good. Predicted sink rates are 7–16% low, while cone angles agree to within 2–4 deg. With the exception of the point at 35% chord, spin rates differ by less than 15%. Note the strong effect of c.g. location on spin rate.

Overall, the results indicate that use of a finite element model for the wing fabric, together with an accounting of flow interference effects from the centerbody, provides a good representation of samara-wing decelerator function. The large differences between predicted and measured spin rates in certain cases remain unexplained, though. Note, in this regard, that for some configurations there may be more than one solution, both physically and mathematically. In any case, further effort directed to the modeling of fabric subjected to this severe environment is certainly warranted. A possible refinement one might consider is a vortex lattice representation of the wing wake, in place of the uniform inflow assumption, accompanied by a more rigorous model of the centerbody wake.

References

[1]Dashcund, D., "IRAAM Wind Tunnel Test—Task III," Avco Systems Div., Rept. AVSD-0343-83-RR, Wilmington, MA, Aug. 1983.

[2]Atkins, J., "Defense Suppression Submunition Program," Avco Systems Textron, Rept. AVST-0093-87-RR, Wilmington, MA, Jan. 1987.

[3]Kline, R., and Koenig, W., "Samara Type Decelerators," AIAA Paper 84-0807, April 1984.

[4]Crimi, P., and Jorgensen, D., "Tests of Samara-Wing Decelerator Characteristics," AIAA Paper 91-0868, April 1991.

[5]Crimi, P., "Analytic Modeling of a Samara-Wing Decelerator," AIAA Paper 86-2439, Oct. 1986.

[6]Crimi, P., "Analysis of Samara-Wing Decelerator Steady-State Characteristics," *Journal of Aircraft*, Vol. 25, No. 1, 1988, pp. 41–47.

[7]Hoerner, S., *Fluid-Dynamic Drag*, published by the author, Brick Town, NJ, 1965, pp. 3–12.

[8]Darling, J., "Handbook of Blunt-Body Aerodynamics, Vol. 1—Static Stability," Naval Ordnance Lab., TR NOLTR 73-225, Silver Spring, MD., Dec. 1973.

[9]Gessow, A., and Myers, G., *Aerodynamics of the Helicopter*, Ungar, New York, 1967, pp. 126–130.

[10]Fail, R., Lawford, J., and Eyre, R., "Low-Speed Experiments on the Wake Characteristics of Flat Plates Normal to an Air Stream," Aeronautical Research Council Reports and Memoranda 3120, London, June 1957.

[11]Critzos, C., Heyson, H., and Boswinkle, R., "Aerodynamic Characteristics of NACA 0012 Airfoil Section at Angles of Attack from 0 to 180 Degrees," NACA TN 3361, Jan. 1955.